Pol. J. Environ. Stud. Vol. 32, No. 2 (2023), 1343-1352
DOI: *10.15244/pjoes/156777* ONLINE PUBLICATION DATE: 2023-01-09

Original Research

Metal Oxide Nanoparticles (Tio_2, Zno, and Fe_2O_3) Change the Functional Groups, but not the Plant Tissue Content of Common Bean Plants Grown in a Greenhouse

César R. Sarabia-Castillo, Andrea Y. Pérez-Moreno, Fabián Fernández-Luqueño*

Sustainability of Natural Resources and Energy Program, Cinvestav-Saltillo, Av. Industria Metalúrgica 1062, Parque Industrial Saltillo-Ramos Arizpe, Ramos Arizpe, Coahuila. C.P. 25900, Mexico

Received: 29 March 2022
Accepted: 21 November 2022

Abstract

The impact of nanoparticles (NPs) on the morphological characteristics, functional groups, and chemical and microstructural features of plant tissues were evaluated using common bean (*Phaseolus vulgaris* L.) plants. Beans plants were grown for 90 days in an agricultural soil amended with TiO_2, ZnO, and Fe_2O_3 NPs at 150 or 300 mg kg^{-1}. Controls consisted of soil without NPs amendments. After 60 days of sowing (DAS), TiO_2 NPs significantly reduced stem and root length compared to control treatments. Additionally, changes were observed in the FTIR- ATR spectra signals, mainly in the root spectra at 30 and 90 DAS. Significant differences were observed in the different plant structures regarding Ti, Zn, and Fe absorption and accumulation. A higher accumulation of Ti was observed in the roots at 90 DAS. Moreover, plants had a higher accumulation of Zn and Fe in leaves, stems, and roots when grown in soil amended with ZnO or Fe_2O_3 NPs, respectively, at 30 and 90 DAS. In the microstructural analysis of tissue showed no evidence of absorption or translocation of NPs. Therefore, the accumulation of ionic forms of Ti, Zn, and Fe in the plant can be explained by the dissociation and dissolution of the NPs in the rhizosphere, facilitating their adsorption.

Keywords: biomass production, crop production, FESEM-EDS, FTIR-ATR, plant tissue, soil pollution, XRD

Introduction

Nanotechnology has emerged as one of the most innovative technologies of this century, which is responsible for developing, manipulating, or controlling matter at the nanometric scale through the precise manipulation of atoms and molecules to design and control nanodevices [1]. The nanotechnology delivers new tools with capabilities that bulk materials do not possess. Furthermore, it allows for less expensive and more profitable development of products for everyday use, including personal care, medical, energy and agricultural products.

*e-mail: fabian.fernandez@cinvestav.edu.mx

A nanomaterial (NM) is any material with at least one of its dimensions on the nanometric scale, i.e., 1 to 100 nm [2]. They can be naturally occurring or they engineered. The latter can include atomic aggregates, nanofibers, nanotubes, fullerenes, thin films, nanocapsules, nanoporous materials, nanowires, dendrimers, quantum dots, nanopowders, and nanoparticles (NPs). The latter are considered zero-dimensional (0-D) materials, i.e., they are composed of three dimensional nanometric particles [3]. Examples of NPs include those of TiO_2, Fe_2O_3, and ZnO, among others. Rapidly increasing availability of products made or containing NPs and their subsequent releases into the environment have heightened concerns about impacts of these particles in receiving ecosystems. NPs can be released into the environment through intentional as well unintentional processes, including combustion, soil erosion, NPs synthesis wastes. Because of their nanometric dimensions they are being able to travel long distances and be deposited in the soil or bodies of water and where they can interact or undergo transformations by organisms present in these ecosystems [4-6].

Inadequate understanding about the possible environmental impacts (positive or negative) of NMs necessitates studies of their behaviors in different ecosystem compartments [7]. For plants, effects of NMs depend on species and size, as well as type, chemical composition, and stability of the NMs. NPs may influence growth, physiology, biochemical traits in plants (for example, the production and quality of edible plants). Furthermore, they can serve as sources of contaminants that enter food chains of living systems [8-10].

Thus, studies have revealed that the possible effects of NMs on the development and growth of various plant species. Several studies reveal that exposure of plants to TiO_2 NPs significantly affects seed germination rate, biomass production, and particularly root development in tobacco (*Nicotiana tabacum* L.), basil (*Ocimum basilicum* L.), and switchgrass (*Panicum virgatum* L.) plants [11-12].

In addition, the exposure to TiO_2 NPs, can cause genetic alterations in plants by decreasing the expression of micro-RNAs responsible for gene regulation in terms of tolerance to abiotic stresses. Furthermore, this type of NPs can decrease the concentration of carbohydrates and chlorophyll in basil plants [12-13].

Similar results were reported by Garcia-Gomez et al. (2018) [14] by exposing plants of maize (*Zea mays* L.), radish (*Raphanus sativus* L.), wheat (*Triticum aestivum* L.), bean (*Phaseolus vulgaris* L.), tomato (*Solanum lycopersicum* L.), lettuce (*Lactuca sativa* L.), pea (*Pisum sativum* L.), cucumber (*Cucumis sativus* L.) and beetroot (*Beta vulgaris* L.) to ZnO NPs. The authors reported that the presence of ZnO NPs altered several parameters related to oxidative stress (chloroplast function and protein content), suggesting a modification in the antioxidant enzyme activity of the plants in response to Zn stress. These results are in agreement with a previous investigation where bean (*Phaseolus vulgaris* var. contender) and cherry tomato (*Solanum lycopersicon* L. var. Cerasiforme) plants were exposed to different Zn sources [15].

In this research, the possible effects of TiO_2, ZnO, and Fe_2O_3 nanoparticles on the growth and development of *Phaseolus vulgaris* L. grown in greenhouses were characterized by studying the morphological, chemical, and microstructural alterations in the plant.

Material and Methods

The present study was carried out in the greenhouse of the Center for Research and Advanced Studies of the National Polytechnic Institute Saltillo unit. Seeds of pinto Satillo bean variety (*Phaseolus vulgaris* L.) were obtained from the Saltillo Experimental Field of the Instituto Nacional de Investigaciones Forestales, Agricolas y Pecuarias (INIFAP).

Nanoparticles, namely, TiO_2, ZnO, and Fe_2O_3 were obtained from 'Investigación y Desarrollo de Nanomateriales S.A. de CV.' The morphology and chemical composition of the three NPs were characterized by field emission scanning electron and energy dispersive X-ray spectrometry (FESEM-EDS) and X-ray diffraction (XRD) (Fig. 1).

Soil Characterization

The soil used in this project was collected from the 'Universidad Autónoma Agraria Antonio Narro' experimental plot. pH, electrical conductivity, bulk density, percentage of organic matter, and texture were determined according to Estefan et al., (2014) [16] The following elements were analyzed: Total P, K, Mn, Mg, Zn, Ca, Fe and Ti by inductively coupled plasma emission spectrometry (ICP-OES, Perkin Elmer; Optima 8300). Additionally, total N was analysed an organic elemental analyzer of dynamic "flash" combustion.

Experimental Setup

Grow bags (30×24 cm) with soil were saturated with tap water and left to drain for three days. After this time, suspensions (in 10 mL of distilled water) of TiO_2, ZnO, or Fe_2O_3 NPs at concentrations of 0, 150, or 300 mg kg^{-1} of dry soil were prepared and added to the soil individually, according to the treatments. There were seven treatments with nine replicates each, which were distributed in a completely randomized design. The replicates without NPs were set as controls.

The seeds were superficially disinfected for sowing in a 70% v/v ethanol solution for 1 minute. They were rinsed twice with sterilized distilled water, followed by a second washing by immersion with 1% v/v sodium hypochlorite for 10 minutes. Finally, they were rinsed twice with sterilized distilled water. Three seeds were

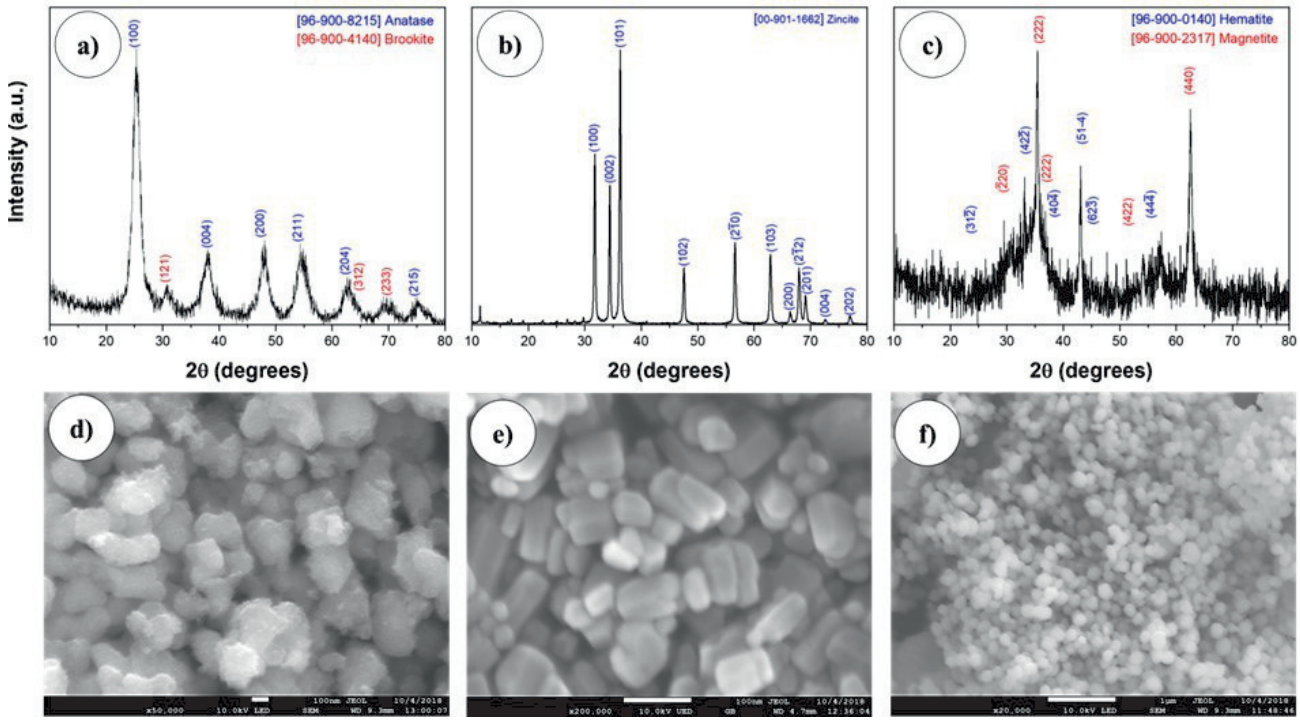

Fig. 1. Characterisation of NPs by XRD and FESEM. XRD patterns and FESEM micrographs of TiO_2 (a and d), ZnO (b and e) and Fe_2O_3 (c and f).

sown in each replicate, and 15 days after sowing (DAS), a thinning was done to maintain only one seedling with uniform size per replicate. The experiment was maintained for 90 days under greenhouse conditions. During this period, three destructive and random samplings were carried out at 30, 60, and 90 DAS.

Sampling and Plant Tissue Analysis

Sampling

At each sampling period, nine plants were chosen at random from each treatment. Three complete plants were used to determine the biomass of the plant. Of the remaining six plants, sample portions of about 5 mm were used for scanning electron microscopy (SEM), and another portion was used for Fourier transform infrared spectroscopy (FTIR) analysis.

Determination of Plant Biomass

Plant biomass was determined by separating the root from the aerial part (stem and leaves). Each section was carefully washed with tap water and then washed with distilled water, and the excess water was allowed to drain off, and the length of the stem and root were measured. Subsequently, the samples were placed separately (root, stem, and leaves) in paper bags and dried in a Thermo Scientific forced air oven at 72ºC for 72 h or until constant weight to determine the dry biomass weight.

Scanning Electron Microscopy

The samples for SEM were immersed separately in a fixative solution (Trump's solution) for 24 h. This solution consisted of 4 mL of 25% purified glutaraldehyde grade I for electron microscopy (Sigma-Aldrich), 10 mL of 37% formaldehyde (Sigma-Aldrich), 1 g of anhydrous monobasic sodium phosphate monobasic (Sigma-Aldrich), 0. 27 g sodium hydroxide (Sigma-Aldrich) and made up to 100 mL with distilled water. For mounting the sample on the stub, the samples were dehydrated at room temperature using a graded ethanol series of 40%, 50%, 60%, 70%, 80%, 90%, and twice at 100% v/v for 30 min at each concentration. After the samples were dehydrated, they were glued to the steel stub with carbon tape and coated with a thin layer of Au/Pd.

Fourier Transform Infrared Spectroscopy

The FTIR samples consisted of root, stem, and leaf segments, which were used without any previous preparation and analyzed in a Perkin Elmer Frontier FTIR spectrometer in a measurement range of 400-4000 cm^{-1}, with a diamond ATR accessory.

Determination of Elemental Concentration

To determine the elemental concentration, the dry tissues obtained from the biomass analysis were used, these tissues were ground until obtaining a fine

powder, separated by treatment and by type of tissue. The obtained powders (root, stem, and leaf powder) underwent a wet acid digestion process as reported by [17], and the elemental concentration (Ti, Zn, and Fe) was measured by inductively coupled plasma emission spectrometry (ICP-OES, Perkin Elmer; Optima 8300).

Statistical Analysis

The data obtained were subjected to analysis of variance (ANOVA) using Minitab 18 software. Tukey's test determined the difference in means at the $p = 0.05$ probability level.

Results and Discussion

Soil Characterization

Table 1 shows characteristics of the soil used in the experiment. Textural analysis shown that the soil is loamy sand, which can provide good aeration for plant growth. It has a high OM content (6.22 %) and a relatively high pH (8.45).

Characteristics of *P. vulgaris* L. Grown in NPs-amended Soil

With only a few exceptions, there were no significant differences in biomass measures due to soil amendment with Ti, Zn, or Fe NPs.

Table 1. Physicochemical characterization of the soil used in this investigation.

Parameter	Result
pH	8.45
Electrical conductivity	531.8 µS cm$\|^{-1}$
Bulk density	0.918 g cm^{-3}
Organic matter content	6.22%
Texture	Loamy sand (72.35% sand, 9.84% clay, and 17.81% silt)
Elemental composition	
P	1.07 g kg^{-1}
K	1.64 g kg^{-1}
Mn	0.099 g kg^{-1}
Mg	2.31 g kg^{-1}
Zn	0.065 g kg^{-1}
Ca	191.2 g kg^{-1}
Fe	6.06 g kg^{-1}
Ti	0.05 g kg^{-1}
N	2.6 g kg^{-1}

Significant differences in root length and steam height were observed for Ti, but this occurred only at 60 DAS. Despite these differences, corresponding dry weights were not different during any sampling period (Table 2). Kibbey and Strevett (2019) [18], reported that the application of TiO_2 NPs at a concentration of 100 mg L^{-1} reduces the length of roots in *Lactuca sativa* L. seedlings. Missaoui et al. (2017) [19], showed that there were no significant effects on the dry stem weights of *Trigonella foenum-graecum* L. plants, as occurred in this investigation.

For Zn and Fe, no significant differences were observed with respect to the control treatment. Nevertheless, studies have revealed that ZnO NPs can cause a decrease in the length of stems and roots of *Medicago sativa* L. [20], in the same way Li et al., (2016) [21] reported the NPs of Fe_2O_3 notably reduce root length in *Zea mays* L.

Scanning Electron Microscopy

In Fig. 2 (a-g), longitudinal sections of stems from the different treatments are shown, in which no structural damage can be seen nor any structure that could be identified as a nanoparticle. However, some semi-spherical structures can be seen, which could be attributed to the presence of starch granules in what could be parenchymal cells because these cells can synthesize and store substances such as sugars, proteins, pigments, etc. The most frequently stored substance in this cell type is carbohydrates in starch [17], which can be observed mainly in the Z300, F150, and F300 treatments (Fig. 2e, 2f, and 2g respectively).

Similarly, the images corresponding to the root sections in Fig. 2 (h-n) do not show damages to microstructure, nor do they show structures that could be related to the presence of NPs inside them. However, as in the stem micrographs, starch granules can also be observed, with a greater quantity seen in the control, T150, T300, Z150, and F300 treatments (Fig. 2h, 2i, 2j, 2k, and 2n, respectively). This is attributed to the fact that some regions of the root cortex where starch granules are more abundant are being observed [22].

Fourier Transform Infrared Spectroscopy

All FTIR-ATR spectra were recorded in the range 500-4000 cm^{-1}. The spectra of fresh leaves of *P. vulgaris* L. from all treatments at 30, 60 and 90 DAS are shown in Fig. 3 (a, d, and g, respectively). These spectra show the presence of functional groups mainly associated with the composition of the leaf cuticle (waxy layer) in the ranges 2852-2914 cm^{-1}, 1739-1728 cm^{-1}, and 1431-1420 cm^{-1} representing the symmetric stretching of the alkyl group (CH_2), carbonyl tension (C=O), and methyl symmetric bending (CH_3) respectively. In the latter, it can be seen that at 30 DAS, the intensity of the band is lower in the control treatment compared to the other treatments, while at 60 DAS this signal

Table 2. Characteristics of bean (*P. vulgaris* L.) plants grown under greenhouse conditions in soil conditioned with TiO_2, ZnO and Fe_2O_3 nanoparticles at concentrations of 150 and 300 mg kg^{-1}.

Characteristic[s]Ω	DAS[ϕ]	Treatment[μ]						
		T150	T300	Z150	Z300	F150	F300	Control
Root length (cm)	30	31.7±5.21[a†]	29.9±4.25[a]	21.7±8.79[ab]	23.5±8.01[ab]	20.1±7.58[b]	23.4±6.43[ab]	22.6±8.44[ab]
	60	39.6±3.15[ab]	33.3±8.34[b]	39.7±6.41[ab]	40.5±4.04[a]	43.2±7.12[a]	46.6±8.17[a]	46.3±3.4[a]
	90	37.5±8.27[a]	32.2±9.51[a]	34.8±11.14[a]	32.0±9.52[a]	39.4±7.19[a]	38.5±7.93[a]	37.1±8.06[a]
Stem height (cm)	30	8.2±1.13[ab]	9.5±1.83[a]	9.0±1.81[ab]	7.7±1.02[ab]	6.9±1.32[b]	8.8±2.12[ab]	8.5±2.34[ab]
	60	13.7±2.84[a]	10.8 ±2.44 [b]	11.7±1.82[ab]	12.3±1.97[ab]	13.1±1.85[ab]	13.7±1.81[a]	14.1 ±1.56[a]
	90	20.0±4.00[a]	14.3±2.56[b]	18.1±2.92[ab]	16.7±3.54[a]	16.5±2.04[ab]	19.4±4.01[a]	15.5 ±2.89[ab]
Root dry weight (g)	30	0.28±0.06[a]	0.17±0.06[a]	0.12±0.02[b]	0.09±0.01[b]	0.06± 0.04[b]	0.13±0.01[b]	0.12±0.04[b]
	60	0.64±0.07[a]	0.55±0.09[a]	0.44±0.11[a]	0.51±0.09[a]	0.56±0.17[a]	0.52±0.13[a]	0.50±0.18[a]
	90	1.22±0.50[a]	0.63±0.13[a]	0.83±0.33[a]	0.42±0.06[a]	0.96±0.32[a]	1.01± 0.56[a]	0.79±0.59[a]
Aerial part dry weight (g)	30	0.38±0.10[a]	0.31±0.03[a]	0.29±0.14[a]	0.22±0.01[a]	0.16 ±0.10[a]	0.31±0.09[a]	0.29±0.06[a]
	60	1.92±0.37[a]	1.30±0.53[a]	1.33±0.58[a]	1.57±0.84[a]	1.62±0.65[a]	1.11±0.17[a]	1.41±0.21[a]
	90	2.32 ±0.84[a]	1.20±0.58[a]	1.50±0.43[a]	1.03±0.11[a]	1.44±0.60[a]	1.91±1.45[a]	1.13±0.52[a]

Ω Root length, and stem height, n = 9; root dry weight and aerial part dry weight n= 3.
ϕ Days after sowing.
μ T150 = TiO_2-NP-150, T300 = TiO_2-NP-300, Z150 = ZnO-NP-150, Z300 = ZnO-NP-300, F150 = Fe_2O_3-NP-150, F300 = Fe_2O_3-NP-300.
† Average values with different capital letters in each row indicate a statistical difference between treatments. (Tukey α = 0.05). Each mean value is accompanied by ± standard deviation.

(1431-1450 cm^{-1}), no longer it is possible to appreciate in the control treatments, Z300, and F300, as well as in the control treatments, Z300 and F300 at 90 DAS. Similarly, in ranges 1540-1533 cm^{-1}, the presence of a signal corresponding to the symmetric bending N-H associated with proteins is observed. This signal can only be seen in the control treatments, T300, Z150, and Z300 at 30 DAS, while at 60 and 90 DAS this signal is no longer observed in any treatments. In addition, the signal corresponding to the bond bending C-O associated with carbohydrate production is observed in the range 1149-1160 cm^{-1} [23-25].

In the spectra of the stems at 30, 60, and, 90 DAS (Fig. 3b, 3e, and 3h), bands attributed to the functional groups of the proteins can be seen, the band corresponding to the tension of the bond C=O in the range of 1634-1610 cm^{-1} [23, 26], which is observed in all treatments at all sampling times, and the band in the range of 1540-4533 cm^{-1} corresponding to the symmetric bending of the bond N-H [26], this signal can only be seen in the F300 treatment at 30 DAS. However, at 60 days this signal can be seen in almost all treatments except for the T150 treatment, but at 90 days this signal is inhibited in the control treatments, T150 and F300. In the 1269-1249 cm^{-1} range, a small signal associated with the phosphate group (P=O) is observed [26], which is slightly appreciated in treatments T300, Z150, F150, and F300 at 30DAS. AT 60 DAS the band is more appreciated in the control treatment, T150, T300, and Z150, and in the treatments T300, Z150, and Z300 at 90 DAS. In addition, in the 1153-1145 cm^{-1} and 1024-1007 cm^{-1} ranges, a signal corresponding to the bending of the C-O bond is shown [23], and an intense signal related to the tension and bending of the bond C-O is shown. These signals can be appreciated in all treatments are all sampling times and are attributed to the carbohydrate composition and is consistent with the micrographs of the stem sections (Fig. 2), where the presence of starch granules can be seen [26].

In the root spectra at 30, 60, and 90 DDS Fig. 3 (c, f, and i, respectively), the positions of some peaks showed some changes compared to the control treatment. For example, the signal at 1417 cm^{-1} is attributed to the symmetric bending of the CH_3 group [23], which is only seen in treatments T150, T300, and Z300 at 30 and in treatments Z300, F150, and F300 at 90 DAS. It could be due to the variation of the chemical conditions of this functional group in the different sampling times.

On the other hand, the signal at 1634 cm^{-1} assigned to the C=O bond stress of primary amides is present in all treatments at each sampling time. At 1030-1020 cm^{-1}, an intense signal corresponding to C-O bond tension and bending can be seen in all treatments. It is attributed to carbohydrate production [26], which, as in the stems, coincides with that observed in the micrographs of the root sections (Fig. 2).

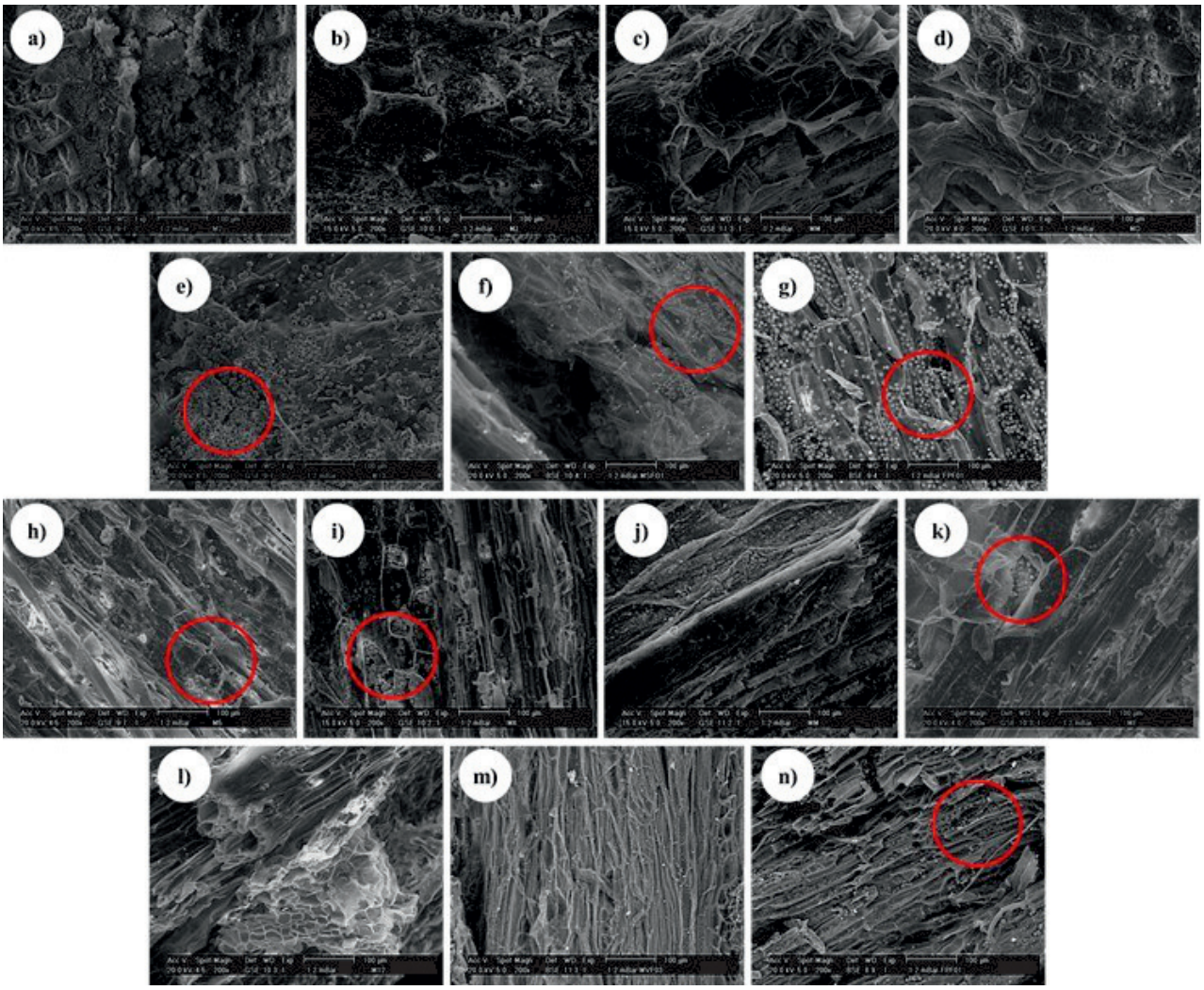

Fig. 2. Micrographs of the internal structure of stems (a-g) and roots (h-n) of *P. vulgaris* L, under different NPs treatments, a) and h) control; b) and i) T150; c) and j) T300; d) and k) Z150; e) and l) Z300; f) and m) F150 and g) and n) F300.

Uptake and Accumulation of NPs in *P. vulgaris* L. Plants

Results of titanium uptake revealed that significantly higher Ti accumulated in roots of *P. vulgaris* L. at 90 DAS compared to control as well as T300 treatments (Table 3). Our observation with Ti accumulation in roots of *P. vulgaris* L. was sil¿milar to that reported by Kelemen et al. (1993) [27], who found similar Ti accumulation in roots of *Triticum aestivum* L. with only little uptakes in leaves. Similarly, Deng et al. (2017) [28], report that Ti accumulation in *Oryza sativa* L. plants occurred to a greater extent in roots, with differences of up to two orders of magnitude compared to Ti accumulation in leaves and stems.

Regarding Zn accumulation in the different tissues of the plant, Table 3 shows that in the case of the leaves at 30 and 90 DAS, the Z150 treatment presented a greater accumulation of zinc than the control. On the other hand, the most significant accumulation of Zn in the stem was found in the Z300 treatment at 30 and 90 DAS, being significantly higher than that of the control treatment. In the case of the roots, it can be observed that at 30 DAS, the accumulation of Zn in the Z300 treatment was significantly higher than that of the control treatment; likewise, at 90 DDS the concentration of Zn in the roots was significantly higher in the Z150 and Z300 treatments compared to the control treatment. From the above and in general, it can be said that the highest accumulation was observed in the root of the plant compared to the concentration of Zn in leaves and stems. This result is consistent with that reported by Zhang et al. (2015) [29], who observed that Zn levels were lower in leaves and stems than in roots in plants of *Schoenoplectus tabernaemontani* (C. C. Gmel.) Palla, exposed to ZnO NPs. According to Lin and Xing (2008) [30], the increase in Zn concentration in roots may be due to the direct interaction of ZnO NPs with roots increasing the adsorption capacity of NPs, preventing them from moving to stems and leaves.

Similarly, in Table 3, it can be observed that the iron accumulation in the leaves was significantly greater in

Table 3. Ti, Zn, and Fe concentration in different sections of common bean plants grown under greenhouse conditions and in soil conditioned with TiO_2, ZnO and Fe_2O_3 nanoparticles at concentrations of 150 and 300 mg kg^{-1} at different sampling times.

Treatment[μ]	Leaf[Ω]			Stem			Root		
	30 DAS[ϕ]	60 DAS	90 DAS	30 DAS	60 DAS	90 DAS	30 DAS	60 DAS	90 DAS
	Ti concentration (mg kg^{-1})								
Control	20.67±9.5[a]	25.17±10[a]	31±9.54[a]	11.33± 0.58[a]	25 ±10.53[a]	2.33±0.58[a]	143.33±11.55[ab]	25±10[a]	340.67±11.02[c]
T150	10.67±4.04[a]	24.33 ±9.71[a]	22.33±8.02[a]	20.67±9.5[a]	25.33± 10.5[a]	3 ±1[a]	150.67±9.71[a]	25.33±10.5[a]	479.67±9.07[a]
T300	10.67±5.03[a]	24±11[a]	27.67±10.01[a]	30.33±11.06[a]	25±10[a]	3.67±0.58[a]	121.33±9.02[b]	24.67±9.61[a]	439±6.08[b]
	Zn concentration (mg kg^{-1})								
Control	40.33± 20.55[b]	47±20.07[a]	54±19.08[b]	28.33±10.41[b]	46±10.54[a]	74.67±10.79[b]	89.67±9.07[c]	135.33±6.11[a]	150.67±8.02[b]
Z150	160 ±9.54[a]	50±9.16[a]	100.67±10.07[a]	50 .33± 9.61[b]	55.67±4.93[a]	80±9[ab]	180±9.54[b]	120.33±9.61[ab]	211.33±10.6[a]
Z300	56.67±6.11[b]	53.67±4.04[a]	65.67±10.07[b]	79.67± 10.02[a]	48±11.14[a]	99.67±9.5[a]	259.67 ±10.02[a]	115.33±7.64[b]	232.33±8.5[a]
	Fe concentration (mg kg^{-1})								
Control	150.33±9.61[b]	49.63±10.06[a]	2.17±1.04[b]	400.33 ±10.6[a]	51.33±9.02[a]	2.03± 1[a]	1700±9.54[a]	39±16.82[a]	1575.33±11.85[c]
F150	139±9.54[b]	50.33±10.6[a]	64±11.14[a]	270±18.5[b]	51±11[a]	1.83±1[a]	140±8.71[c]	50.67±9.02[a]	2512±10.15[b]
F300	199±9.54[a]	49.5±10.26[a]	84.83±9.8[a]	149±9.54[c]	51±10.54[a]	2.2±1[a]	1120±9.02[b]	49.33±9.5[a]	2597.67±7.64[a]

[Ω] n = 3.

[ϕ] Days after sowing.

[μ] T150 = TiO_2-NP-150, T300 = TiO_2-NP-300, Z150 = ZnO-NP-150, Z300 = ZnO-NP-300, F150 = Fe_2O_3-NP-150, F300 = Fe_2O_3-NP-300.

[†] Mean values with different letters in each row indicate a statistical difference between treatments. (Tukey p = 0.05). Each mean value is accompanied by±standard deviation.

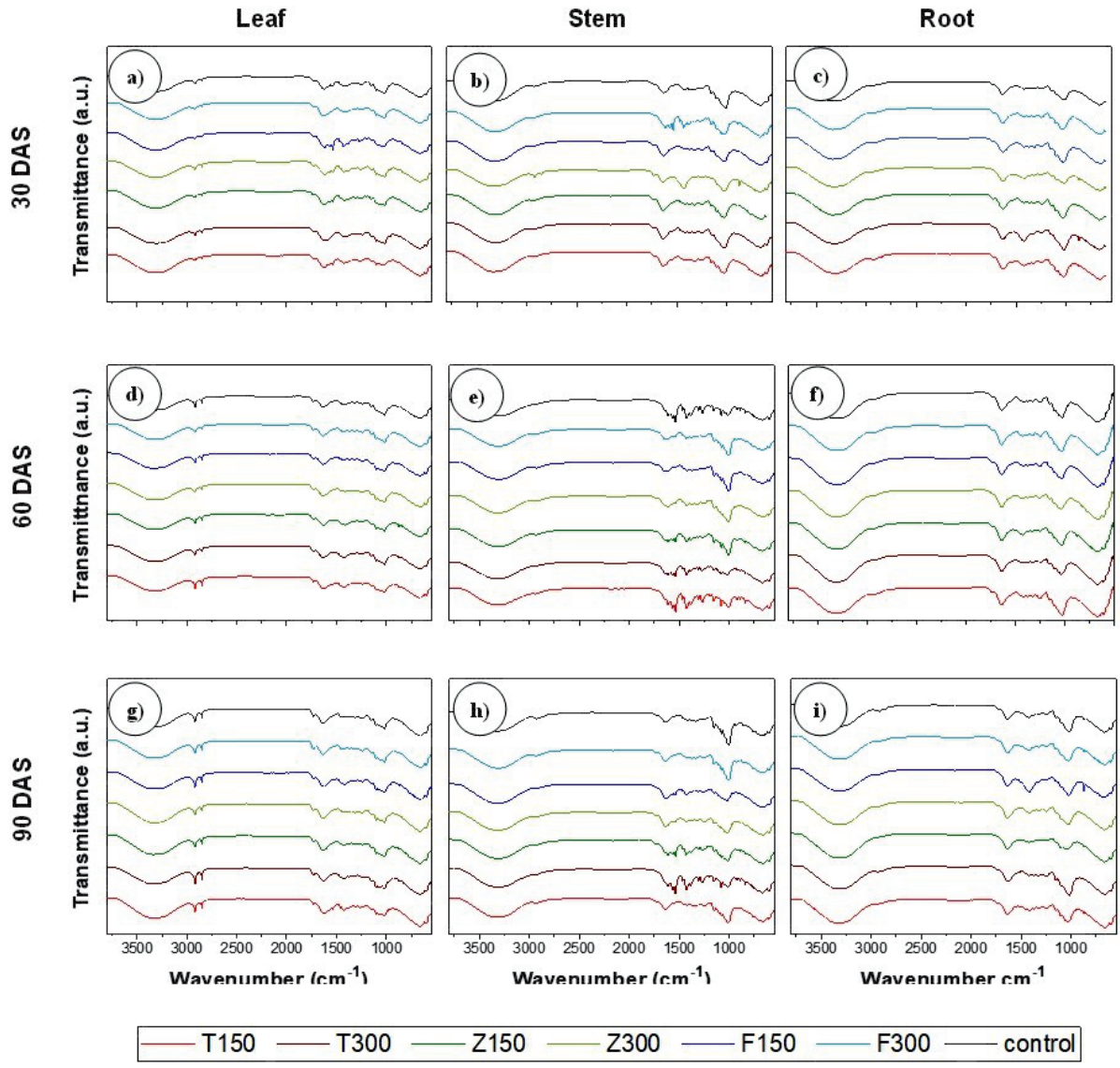

Fig. 3. Infrared spectra of fresh leaves (a, d and g), stems (b, e and h) and roots (c, f and i) of common bean. a)-c) 30 DAS, d)-f) 60 DAS and g)-i) 90 DAS.

the F300 treatment compared to the control treatment at 30 DAS. Likewise, at 90 DAS it could be observed that Fe accumulation was significantly higher in F150 and F300 treatments compared to control treatment.

The accumulation of Fe in the stems at 30 DAS was significantly lower in the treatments F300 and F150 compared to the control treatment. On the other hand, the content of Fe in the roots at 30 DAS was significantly lower in the treatments F300 and F150 compared to the control treatment, being the treatment F150 the one that accumulated less Fe in the roots. However, at 90 DAS, it was observed that Fe content was significantly higher in F150 and F300 treatments compared to control treatment, with F300 being the treatment with the highest Fe content in the roots at this sampling time.

It is in concordance with Al-Amri et al. (2020) [31], who found that the greatest accumulation of Fe in plants of *T. aestivum* L. exposed to Fe_2O_3 NPs, occurs in the roots obtaining less accumulation in the leaves. However, in a previous study conducted by Pariona et al. (2017) [32], they found that the greatest accumulation of Fe in plants of *Quercus macdougallii* Martínez, exposed to Fe_3O_4 NPs occurs in the leaves of this plant so that the NPs accumulation may depend on the ability to uptake and transport metals from the roots to the aerial parts such as stems and leaves of each specific plant.

Conclusions

The application of TiO_2 NPs significantly modified the growth of *P vulgaris* L. plants by reducing the length of the root and stem of the plants. Changes in the functional groups of *P. vulgaris* L. plants were detected. These changes were mostly observed in the

root sections because roots have greater interaction with the NPs when soil is directly amended with NPs.

Use of FTIR-ATR analysis can provide knowledge about changes in physiological and biochemical interactions between NPs and plants. In turn, this can lead to a better understanding of plant responses to exposures to anthropogenically-mediated abiotic agents in ecosystem compartments.

Metal accumulation in the plant biomass increased because of transformation or dissolution of the metallic NPs during the exposure period. As evidenced by ICP-OES, the presence of metals in plant tissues was consistent with rhizosphere-facilitated dissolution, absorption and translocation of Ti, Zn, and Fe in their ionic form by the plants.

Acknowledgments

This research was founded by the projects 'Ciencia Básica SEP-CONACyT-151881', 'FONCYT-COAHUILA COAH-2019-C13-C006', and 'FONCYT-COAHUILA COAH-2021-C15-C095', by the Sustainability of Natural Resources and Energy Program (Cinvestav-Saltillo), and by Cinvestav Zacatenco.

Conflict of Interest

The authors declare no conflict of interest.

References

1. BAYDA S., ADEEL M., TUCCINARDI T., CORDANI M., RIZZOLIO F. The history of nanoscience and nanotechnology: from chemical-physical applications to nanomedicine. Molecules, **25** (1), 112, **2019**.
2. BAIG N., KAMMAKAKAM I., FALATH W. Nanomaterials: a review of synthesis methods, properties, recent progress, and challenges. Materials Advances, 2 (6), 1821, **2021**.
3. POKROPIVNY V.V., SKOROKHOD V.V. Classification of nanostructures by dimensionality and concept of surface forms engineering in nanomaterial science. Materials science and engineering: C, **27** (5-8), 990, **2007**.
4. VALLE-GARCIA J.D., SARABIA-CASTILLO C.R., PEREZ-HERNANDEZ H, TORRES-COMEZ A.P., PEREZ-MORENO A., FERNANDEZ-LUQUEÑO F. Chapter 8 - Influence of nanoparticles on the physical, chemical, and biological properties of soils. A. Amrane, D. Mohan, T.A. Nguyen, A.A. Assadi, G. Yasin (Eds.), Nanomaterials for Soil Remediation, Elsevier, 151, **2021**.
5. LAHIANI M.H., KHODAKOVSKAYA M.V. Concerns about nanoparticle hazard to human health and environment. C. Kole, D.S. Kumar, M.V. Khodakovskaya (Eds.), Plant Nanotechnology: Principles and Practices. Springer. 349, **2016**.
6. SHUKLA P.K., MISRA P., KOLE C. Uptake, translocation, accumulation, transformation, and generational transmission of nanoparticles in plants. C. Kole, D.S. Kumar, M.V. Khodakovskaya (Eds.), Plant Nanotechnology: Principles and Practices. Springer183, **2016**.
7. RICO C.M., HONG J., MORALES M.I., ZHAO L., BARRIOS A.C., ZHANG J.Y., PERALTA-VIDEA J.R., GARDEA-TORRESDEY J.L. Effect of cerium oxide nanoparticles on rice: a study involving the antioxidant defense system and in vivo fluorescence imaging. Environmental Science and Technology, **47** (11), 5635, **2013**.
8. ZARATE-CRUZ G.S., ZAVALETA-MANCERA H.A., ALARCÓN A., JIMÉNEZ-GARCÍA L.F. Fitotoxicidad de nanopartículas de ZnO en el helecho acuático *Azolla filiculoides* Lam. Agrociencia, **50** (6), 677, **2016**.
9. ZUVERZA-MENA N., MARTÍNEZ-FERNÁNDEZ D., DU W., HERNANDEZ-VIEZCAS J.A., BONILLA-BIRD N., LÓPEZ-MORENO M.L., KOMÁREK M., PERALTA-VIDEA J.R., GARDEA-TORRESDEY J.L. Exposure of engineered nanomaterials to plants: Insights into the physiological and biochemical responses-A review. Plant Physiology and Biochemistry, **110**, 236, **2017**.
10. BALÁŽOVÁ Ľ., BABULA P., BALÁŽ M., BAČKOROVÁ M., BUJŇÁKOVÁ Z., BRIANČIN J., KURMANBAYEVA A., SAGI M. Zinc oxide nanoparticles phytotoxicity on halophyte from genus *Salicornia*. Plant Physiology and Biochemistry, **130**, 30, **2018**.
11. FRAZIER T.P., BURKLEW C.E., ZHANG B. Titanium dioxide nanoparticles affect the growth and microRNA expression of tobacco (*Nicotiana tabacum*). Functional and Integrative Genomics, **14** (1), 75, **2014**.
12. BOYKOV I.N., SHUFORD E., ZHANG B. Nanoparticle titanium dioxide affects the growth and microRNA expression of switchgrass (*Panicum virgatum*). Genomics, **111** (3), 450, **2019**.
13. TAN W., DU W., BARRIOS A C., ARMENDARIZ R., ZUVERZA-MENA N., JI, Z., CHANG C.H., ZINK J.I., HERNANDEZ-VIEZCAS J.A., PERALTA-VIDEA J.R., GARDEA-TORRESDEY J.L. Surface coating changes the physiological and biochemical impacts of nano-TiO_2 in basil (*Ocimum basilicum*) plants. Environmental Pollution, **222**, 64, **2017**.
14. GARCÍA-GÓMEZ C., OBRADOR, A., GONZÁLEZ D., BABÍN M., FERNÁNDEZ M.D. Comparative study of the phytotoxicity of ZnO nanoparticles and Zn accumulation in nine crops grown in a calcareous soil and an acidic soil. Science of The Total Environment, **644**, 770, **2018**.
15. GARCÍA-GÓMEZ C., OBRADOR A., GONZÁLEZ D., BABÍN M., FERNÁNDEZ M.D. Comparative effect of ZnO NPs, ZnO bulk and $ZnSO_4$ in the antioxidant defences of two plant species growing in two agricultural soils under greenhouse conditions. Science of The Total Environment, **589**, 11, **2017**.
16. ESTEFAN G., SOMMER R., RYAN J. Analytical methods for soil-plant and water in the fry areas. A manual of relevance to the west Asia and North Africa region, 3rd Ed; International Center for Agricultural Research in the Dry Areas, Aleppo, 255, **2014**.
17. PEQUERUL A., PÉREZ-RONTOMÉ C., MADERO P., VAL J., PACHECO E.A Rapid wet digestion method for plant analysis. Optimization of Plant Nutrition, 3, **1993**.
18. KIBBEY T.C.G., STREVETT K.A. The effect of nanoparticles on soil and rhizosphere bacteria and plant growth in lettuce seedlings. Chemosphere, **22**, 703, **2019**.
19. MISSAOUI T., SMIRI M., CHMINGUI H., HAFIANE A. Effects of nanosized titanium dioxide on the photosynthetic metabolismo f fenugreek (*Trigonella foenum-graecum* L.). Comptes rendus biologies, **340** (11-12), 499, **2017**.

20. WANG X., WU P., ZHOU C., LI L., BIN-ZHAO Y., CHEN Y. Effect of ZnO nanoparticles on *Medicago sativa* at the germination stage. Applied Mechanics and Materials, **665**, 583, **2014**.
21. LI J., HU J., MA C., WANG Y., WU C., HUANG J., XING, B. Uptake, translocation and physiological effects of magnetic iron oxide (γ-Fe_2O_3) nanoparticles in corn (*Zea mays* L.). Chemosphere, **159**, 326, **2016**.
22. LOZA-CORNEJO S., APARICIO-FERNANDEZ X., PATAKFALVI R.J., ROSAS-SAITO G.H. Caracteres anatómicos y fitoquímicos del tallo y raíz de *Mammillaria uncinata* (Cactaceae). Acta Botánica Mexicana, 21. **2017**.
23. SURESH S., KARTHIKEYAN S., JAYAMOORTHY K. FTIR and multivariate analysis to study the effect of bulk and nano copper oxide on peanut plant leaves. Journal of Science: Advanced Materials and Devices, **1** (3), 343, **2016**.
24. WARREN F.J., PERSTON B.B., GALINDEZ-NAJERA S.P., EDWARDS C. H., POWELL P.O., MANDALARI G., CAMPBELL G.M., BUTTERWORTH P.J., ELLIS P.R. Infrared microspectroscopic imaging of plant tissues: spectral visualization of *Triticum aestivum* kernel and *Arabidopsis* leaf microstructure. The Plant Journal, **84** (3), 634, **2015**.
25. PEÑA L., RENTERÍA V., VELÁSQUEZ C., OJEDA ML., BARRERA E. Absorbancia y reflectancia de hojas de *Ficus* contaminadas con nanopartículas de plata. Revista Mexicana de Física, **65** (1), 95, **2019**.
26. BARRAZA-GARZA G., DE LA ROSA L.A., MARTÍNEZ-MARTÍNEZ A., CASTILLO-MICHEL H., COTTE M., ALVAREZ-PARRILLA E. La microespectroscopía de infrarrojo con transformada de Fourier (FTIRM) en el estudio de sistemas biológicos. Revista Latinoamericana de Química, **41** (3), 125, **2013**.
27. KELEMEN G., KERESZTES A., BACSY E., FEHER M., FODOR P., PAIS I. Distribution and intracellular localization of titanium in plants after titanium treatment. Food Structure, **12** (1), 67, **1993**.
28. DENG Y., PETERSEN E.J., CHALLIS K.E., RABB S.A., HOLBROOK R.D., RANVILLE J.F., NELSON B.C., XING B. Multiple Method Analysis of TiO_2 Nanoparticle Uptake in Rice (*Oryza sativa* L.) Plants. Environmental Science and Technology, **51** (18), 10615, **2017**.
29. ZHANG D., HUA T., XIAO F., CHEN C., GERSBERG R.M., LIU Y., STUCKEY D., NG W.J., TAN S.K. Phytotoxicity and bioaccumulation of ZnO nanoparticles in *Schoenoplectus tabernaemontani*. Chemosphere, **120**, 211, **2015**.
30. LIN D., XING B. Root Uptake and Phytotoxicity of ZnO Nanoparticles. Environmental Science and Technology, **42** (15), 5580, **2008**.
31. AL-AMRI N., TOMBULOGLU H., SLIMANI Y., AKHTAR S., BARGHOUTHI M., ALMESSIERE M., ALSHAMMARI T., BAYKAL A., SABIT H., ERCAN, I., OZCELIK S. Size effect of iron (III) oxide nanomaterials on the growth, and their uptake and translocation in common wheat (*Triticum aestivum* L.). Ecotoxicology and Environmental Safety, **194**, 110377, **2020**.
32. PARIONA N., MARTÍNEZ A.I., HERNANDEZ-FLORES H., CLARK-TAPIA R. Effect of magnetite nanoparticles on the germination and early growth of *Quercus macdougallii*. Science of the Total Environment, **575**, 869, **2017**.